

Experimental Observation of Induced Thermochromic Effect and Nematic Defects in Hydrogen Bonded Liquid Crystals

T. VASANTHI^a, V BALASUBRAMANIAN^b,
S. RADJAREJESRI^b AND V.N. VIJAYAKUMAR^{a,*}

^a*Department of Physics, Condensed Matter Research Laboratory (CMRL),
Bannari Amman Institute of Technology, Sathyamangalam 638 401, India*

^b*Department of Science, Sona College of Technology, Salem 636 005, Tamil Nadu, India*

Received: 10.11.2020 & Accepted: 10.01.2021

Doi: [10.12693/APhysPolA.139.139](https://doi.org/10.12693/APhysPolA.139.139)

*e-mail: vnvphysics@gmail.com

Hydrogen bonded liquid crystal mixtures are derived from: (i) non-mesogenic compounds of diglycolic acid (DGA), (ii) mesogenic compounds of 4-amyloxybenzoic acid (5OBA) and (iii) 4-hexyloxy benzoic acid (6OBA). The existence of intermolecular H-bond is confirmed with FTIR and validated using the density functional theory studies. Polarized light microscopy and differential scanning calorimetry are used to observe the phase variations and transition temperature. In addition, enthalpy values of different mesogenic phases are determined. It is worth mentioning that the nematic mesogenic defects with $S = \pm 1$ and $S = +1/2$ are also analyzed. In order to discuss the induced higher order smectic F phase and its stability, the density functional theory study is applied. The band gap energy of the hydrogen bonded liquid crystal mixtures is found to be 5.1780 eV, based on the HUMO–LUMO approach. This induced thermochromic effect of hydrogen bonded liquid crystal mixtures is a useful phenomenon that can be utilized in optical device applications. In this paper, variation on liquid crystal parameters as well as the formation of H-bond between an acceptor and a donor, along with the extension of a chain length, are also reported.

topics: nematic defect, smectic F, thermochromic effect, POM

1. Introduction

Among soft materials, a liquid crystal (LC) is unique and characterized by the molecular order and its mobility [1]. LC is an efficient material used in the transportation of molecules, sensors and catalysts. The existence of the self-assembling property in an LC molecule, such as weak interaction of H-bonding, π – π stacking, charge transfer mechanism and dipolar interactions etc., plays a vital role in the fabrication of LC devices [1, 2]. An interrelation between the molecular structure exhibits mesomorphism in an LC complex [3]. Kato and Frechet [4] reported that novel supramolecular LCs were obtained by the molecular recognition through intermolecular H-bonds. A novel mesophase is induced in the binary mixture through an H-bond interaction between two different molecules [5, 6].

An interruption in the LC molecular alignment, direction and topological arrangement may cause defects in mesophases. Generally, a defect is found experimentally in an isolated point or disclination line [7]. The defect plays an important role in condensed matter materials because it is used to calculate the potential, efficiency, optical property and

electrical conductivity of the materials [8]. During the phase transition, the molecular order breaks down [9] or is kinetically captured. The color change in thermotropic LCs was reported by various research groups [10, 11]. The reversible thermochromic effect was observed for Schiff base substitute complexes [12]. The thermochromic effect was recognized in polydiacetylene for a bio-sensing activity during heating and cooling [13]. Changeable chromic characteristics were evaluated for organic materials due to their lowest discoloration temperature and their wide applications [14]. Thermochromic LCs were calibrated to identify the relation between color and temperature for the accurate measurement [15]. Due to their degradable nature, some of thermochromic liquid crystals (TLCs) are not stable [16, 17]. A thermochromic effect in LC materials is mainly used in printing technology, military, textiles [18, 19], bio-medical and electro-optical device applications [20]. Abdullah et al. [15] reported that TLCs were mostly used in a thermal imaging tool and the heat transfer mechanism. From the optimized geometry, we can identify various parameters and they are compared with the hypothetical methods using the density functional theory (DFT) [21–23].

With our previous knowledge concerning the design, synthesis and characterization of single [24], double [25] and multiple hydrogen bonded liquid crystals [26], a successful attempt has been made to characterize the DGA+nOBA ($n = 5$ and 6) hydrogen bonded liquid crystals (HBLCs). Also, the experimental values are compared with theoretical DFT calculations. In this paper, we mainly focused on the induced thermochromic effect and nematic defects in the DGA+nOBA ($n = 5$ and 6) HBLC mixture.

2. Materials and methods

A non-mesogenic compound of DGA and mesogenic compounds of 5OBA and 6OBA were obtained from Sigma Aldrich, Germany, and an E. Merck grade solvent was used. The mesomorphic textural changes and their phase transition temperatures were recorded by an Olympus polarized optical microscope (POM) connected to a Sony CCD.17.UH310 USB CCD 3.1MP camera. Further, POM was interconnected with an MHCS400 (MicroOptik) hot and cold stage temperature controller with a resolution of $\pm 0.1^\circ\text{C}$, using MTDC600 software. The enthalpy value for the corresponding mesophase was obtained by a differential scanning calorimeter (DSC, Shimadzu DSC-60Plus with TA60 software, version 2.21). A FTIR spectrum was recorded for the DGA+6OBA mixture using ABB FTIR, MB3000. Gaussian 09 package was used to perform DFT studies. The basis set of B3LYP/6-311G (d, p) was used to optimize the DGA+6OBA double HBLC mixture.

2.1. Preparation of DGA+nOBA HBLC mixture

The dimeric nature of 4-*n*-alkoxybenzoic acid (*n*OBA) was converted to a monomer using excess tetrahydrofuran (THF) and *n*OBA ($n = 5, 6$) was dissolved (separately) in THF and stirred for 12 h with 750 rpm, using a magnetic stirrer. A white crystalline compound of *n*OBA was obtained. Also,

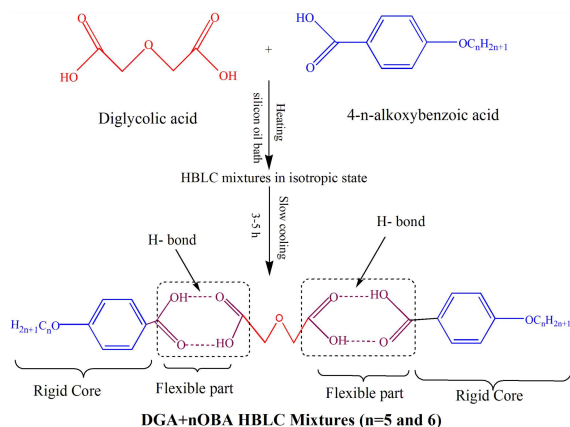


Fig. 1. Molecular structure of the DGA+nOBA ($n = 5$ and 6) hydrogen bonded LC mixture.

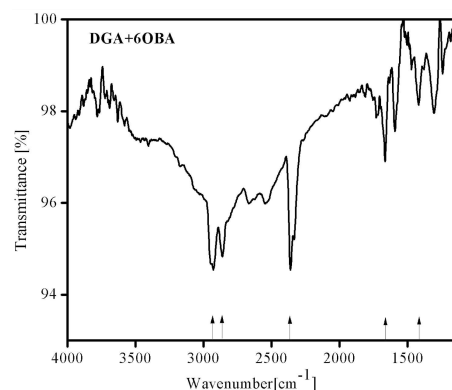


Fig. 2. FTIR spectra of the DGA+6OBA hydrogen bonded LC mixture.

DGA and *n*OBA monomers were appropriated in a 1:2 mole ratio and the mixture was kept in a silicon oil bath by melting the proper amount of mixture above their clearing point. Then, slowly cooled for 3 to 5 h at an ambient temperature, a white crystalline HBLC mixture was obtained as an end product. The molecular structure of DGA+nOBA and its preparation is depicted in Fig. 1.

3. Results and discussion

3.1. Experimental studies on FTIR

The FTIR spectrum was an important tool in determining the functional group and its corresponding vibrational mode. Stretching frequencies of the DGA+6OBA HBLC mixture were experimentally studied. The formation of a hydrogen bond itself was confirmed by experimental FTIR studies (see Fig. 2). In [27], it was reported that a C=O stretching vibration was observed at 1685 and 1695 cm^{-1} . In [28], an aromatic stretching vibration of C–H was reported at 3100–3000 cm^{-1} . In the case of the DGA+6OBA HBLC mixture, a C=O stretching vibration was noticed at 1668 cm^{-1} , the alkyl group (C–H) stretching frequency was observed at 2362 cm^{-1} and 2864 cm^{-1} , while a sharp peak of a $\nu(\text{O–H})$ stretching vibration was noticed at 2939 cm^{-1} .

3.2. Optical studies

The prepared HBLC mixtures were highly stable at room temperature of around 30°C which was confirmed using repeated thermal scanning. The mesophase transition and the respective textural changes were recorded using a CCD camera connected to a POM. Its transition temperature was controlled by a MicroOptik temperature controller. The DGA+nOBA ($n = 5$ and 6) HBLC mixture exhibits different characteristic textures, i.e., schlieren texture with a defect (nematic) and mosaic texture (Sm F). This result was compared with the texture reported in [29]. The phase transition temperature (see Table I) as well as its corresponding textures are shown in Fig. 3.

Mesophase transition temperature and corresponding enthalpy values of the DGA+nOBA ($n = 5$ and 6) HBLC mixture. H — heating, C — cooling, N — nematic, F — Sm F

TABLE I

HBLC mixtures	Mesophase variance	Study	Cycle	Cry. to melt	Nematic	Sm F	Crystal
DGA+5OBA	NF	POM	H	123.3°C	149.4°C	145.3°C	
			C		148.4°C	144.7°C	115.2°C
		DSC	H	122.2°C (53.48 J/g)	148.3°C (1.32 J/g)	144.4°C (1.22 J/g)	
			C		147.5°C (1.05 J/g)	143.8°C (3.69 J/g)	114.1°C (44.9 J/g)
DGA+6OBA	NF	POM	H	104.3°C	150.6°C	146.9°C	
			C		148.9°C	145.9°C	94.6°C
		DSC	H	104.2°C (41.78 J/g)	149.7°C (2.29 J/g)	145.7°C (3.03 J/g)	
			C		147.5°C (2.50 J/g)	144.4°C (1.65 J/g)	93.2°C (37.81 J/g)

In the DGA+nOBA HBLC mixture, the nematic defects were experimentally viewed using POM. The elastic constant has a distinct orientation order and its magnitude is smaller than that of the crystal. Therefore, the defects increase not only in the order of a certain atomic distance but they can also be measured in micrometers. Figure 3a represents the singularity with two- and four-brush nematic schlieren defects. Similarly, the schlieren texture of the nematic phase with two and four-brush defects was reported in [30]. The defect appeared in the central core which has two or four darkened regions which are called brushes.

The defect region was black because the order parameter S is zero at that particular point. Also, the nematic brush was black since its field director (n) is parallel or perpendicular to the analyzer and polarizer. Schlieren defects have strength (s) and their sign denotes the number of brushes divided into four segments. The sign also depends on the director, the lengthy axis of the spatial and the direction of orientation. The sign determination was done by the rotation of the LC sample between two crossed polarizers. When the nematic brush rotates in the clockwise direction, it becomes positive, whereas the negative sign denotes the anticlockwise direction. While the synthesized HBLC mixture was observed under the crossed polarizer, the binary mixture shows a line defect visualization strength of $S = +1$, $S = -1$ and $S = +1/2$. A similar disclination strength, however, with four values, i.e., $S = \pm 1, \pm 1/2$, was reported, e.g., in [31–34]. Importantly, two and four brushes were identified due to the symmetry breaking.

Thermochromic changes (primary RGB color) in nematic with two- and four-brush defect are displayed in Fig. 3b and c. In the HBLC mixtures, the nematic defect phase was related to the thermal dissimilarity. Due to its thermal agitation, the reorientation of the molecule disturbs the refractive index

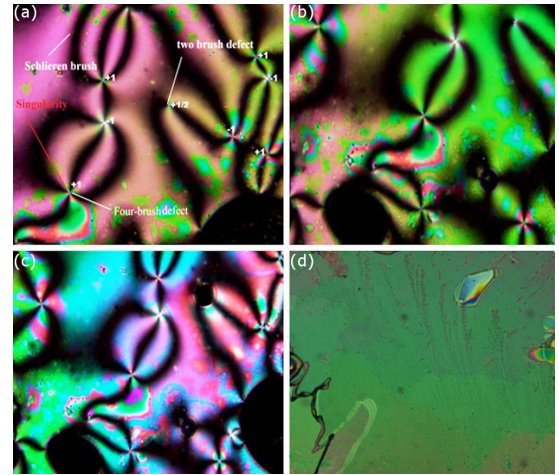


Fig. 3. Mesogenic textures of the DGA+nOBA ($n = 5$ and 6) HBLC mixture: (a) schlieren texture of nematic with two- and four-brush defect, (b) thermochromic change of nematic with two- and four-brush defect, (c) RGB color of nematic with two- and four-brush defect, (d) mosaic texture of SmF.

which, in turn, induces thermochromic changes in the DGA+nOBA HBLC mixture. As the temperature decreases, the primary colors texture, such as red, green and blue, is observed, as shown in Fig. 3c. It should be noted here that the temperature variation is accurately identified with respect to the colors. Thus, such a kind of thermochromic effect can be very useful in medical and optoelectronic device applications, such as optical filters, polarizing filters and heat transfer applications. On further cooling, the nematic schlieren defect is turned to a higher order Sm F phase (see Fig. 3d) with a mosaic texture and finally reaches the crystal. The phase sequence of DGA+nOBA ($n = 5$ and 6) is given below

$$\text{Iso} \rightleftharpoons \text{N} \rightleftharpoons \text{Sm F} \leftarrow \text{crystal}. \quad (1)$$

3.3. Thermal studies

In the case of the HBLC mixture, the mesophases transition temperature and its enthalpy values are depicted in Table I. As the enthalpy value < 1 , the first order transition from the isotropic to nematic phase was observed. Figure 4 represents the DSC thermogram of DGA+nOBA for $n = 5$ and 6 at the scan rate of $5^\circ\text{C}/\text{min}$. These compounds exhibit three endothermic and exothermic peaks. Transition temperatures of corresponding phases are validated with the POM results and found to be the same in both cases, $n = 5$ and $n = 6$.

The thermal span width of nematic and Sm F phase was determined from the DSC spectrum in a cooling cycle. The span width of nematic and Sm F phase of DGA+5OBA was revealed to be 3.7 and 29.7, respectively. Similarly, the nematic and Sm F span width for DGA+6OBA was observed as 3.15 and 51.25, respectively. When the alkoxy chain number increases in the HBLC mixture, the thermal span width also increases (Sm F phase). Note that this Sm F is a higher order phase because its molecular orientation is tilted to the side of its hexagon. This result clearly indicates the appearance of the higher order phases at the lower temperature. In the DSC thermogram, the origination of the crystal in the HBLC mixture was indicated by a sharp peak whereas its corresponding phase changes were recognized in POM studies.

In the cooling and heating cycle, two phases are observed for both $n = 5$ and 6 of DGA+nOBA. However, an additional peak represents crystal to crystal transition in the DGA+6OBA HBLC during the heating cycle due to the rearrangement of molecules near the critical temperature.

3.4. Phase stability factor

Phase stability typically depends on the thermal phase width of the LC phases [35, 36]. Also, it is a significant LC parameter to identify the efficient material for optical device fabrications.

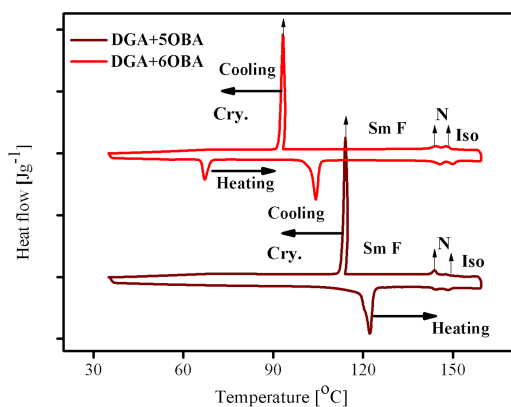


Fig. 4. DSC thermogram for the DGA+nOBA ($n = 5$ and 6) HBLC mixture.

TABLE II

Phase stability for the DGA+nOBA ($n = 5$ and 6) HBLC mixture.

HBLC mixtures	Nematic	Sm F
DGA+5OBA	539	3810
DGA+6OBA	459	6087

The mesophase transition temperature is affected by two symmetric end chains [37]. An individual LC phase and its significance were studied by the calculation of the phase stability factor [38]. The DGA+6OBA HBLC mixture was a representative case in which Sm F was discussed for phase stability factor. Phase stability increases from the nematic to the Sm F phase due to pseudo-hexagonal molecular packing with long-range positional ordering. The stability factor of the Sm F phase was given by

$$S_F = T_{\text{mid}} \Delta T_F, \quad (2)$$

where T_{mid} is the average transition temperature of SmF and crystal phase; ΔT_F is the Sm F thermal range. Based on the results shown in Table II, it becomes clear that the nematic phase possesses lower thermal stability than the Sm F phase. The increasing chain length in the HBLC mixture and steric hindrance influence the thermal stability.

4. DFT studies

4.1. Optimized geometry and frontier molecular orbital

The DGA+6OBA mixture shown in Fig. 5a-c was optimized using the correlation function (B3LYP). The same was used to analyze the H-bond angle (see Fig. 5b) and bond length (see Fig. 5c), and dihedral angle and its dipole moment. According to [39], the molecule had a stable potential energy which was derived from the optimized geometry. The molecular interaction of DGA+6OBA, $\text{O}_{37} \dots \text{H}_{81}-\text{O}_{50}$, $\text{O}_{51} \dots \text{H}_{47}-\text{O}_{35}$, $\text{O}_2 \dots \text{H}_{33}-\text{O}_2$ and $\text{O}_{36} \dots \text{H}_{48}-\text{O}_3$ are shown in Fig. 5a.

Chemical properties were calculated by frontier molecular orbital studies [40, 41]. From the HOMO and LUMO studies, dynamic stability and optical absorption of the HBLC mixture has been obtained [42]. The band gap energy of the DGA+6OBA HBLC mixture was calculated to be 5.1780 eV (see Fig. 6). This mixture shows a higher stability of the present HBLC mixture. Using Koopman's equation [43], the chemical descriptors electron negativity $\chi = 3.888$ eV, the chemical potential $\mu = -3.888$ eV, the global hardness $\eta = 2.589$ eV, the global softness $s = 0.1931$ eV, the maximum electronic charge $\Delta_{n \text{ max}} = 1.501$ eV, the global electrophilicity index $\omega = 2.919$ eV and the total dipole moment 0.8182 D for the DGA+6OBA HBLC mixture were calculated. The existence of lower global softness shows that the HBLC molecule

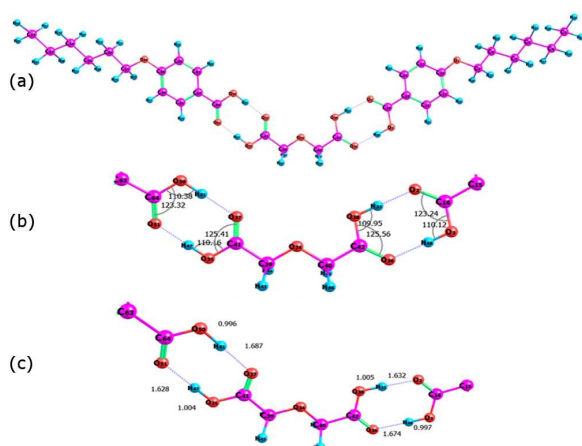


Fig. 5. Optimized geometry of the DGA+6OBA of HBLC mixture.

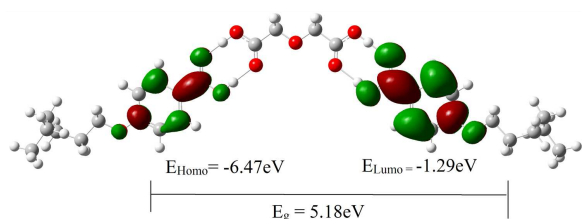


Fig. 6. HOMO-LUMO band gap energy of the DGA+6OBA HBLC mixture.

has a soft nature. In HOMO-LUMO studies, it was found that the bandgap energy increases while increasing the phase stability in the Sm F. Similarly, the highest bandgap energy shown is a clear evidence for the chemically stable HBLC mixture. Also, the same was experimentally proved by repeated thermal scanning performed using DSC at a different scanning rate.

4.2. Binding energy of intermolecular hydrogen bond in DGA+6OBA mixture

In the HBLC mixture (DGA+6OBA), the H-bond was identified between O-H—O bonding. It was already reported [44] that the H-bonding formation energy considerably reflects the strength of O-H—O bond which affects the phase stability and mesophases transition temperature range. Therefore, to compute the binding energy of the DGA+6OBA HBLC mixture by the DFT method, one uses

$$\Delta E = E_{AB} - (E_A + E_B) \quad (3)$$

or

$$E_{\text{bind}} = E_{\text{opt}}^{\text{dim}} - (E_{\text{opt}}^{\text{mon1}} + E_{\text{opt}}^{\text{mon2}}), \quad (4)$$

where E_{AB} — the total energy of the DGA+6OBA dimer, E_A — the total energy of the DGA monomer and E_B — the total energy of 6OBA monomer.

The corrected binding energy of the DGA+6OBA mixture is then

$$\Delta E' = E_{AB} - (E'_A + E'_B). \quad (5)$$

The corrected energy $\Delta E'$ and dissociation energy ΔE are calculated to the basis set superposition error, namely

$$\text{BSSE} = \Delta E' - \Delta E. \quad (6)$$

From the optimization, the uncorrected energy was found to be -1996.618 a.u., whereas the counterpoise corrected energy was obtained as -1996.425 a.u. In the DGA+6OBA HBLC mixture, the counterpoise dissociation energy was calculated as -22.61 kcal/mol, whereas the binding energy -19.27 kcal/mol and BSSE energy 3.34 kcal/mol. Fedorov et al. reported [45] that $A_1 \dots B_1$, $A_2 \dots B_2$ and $A_3 \dots B_3$ complexes had strong intermolecular H-bond. Similarly, in DGA+6OBA, the calculated binding energy clearly reveals the existence of a strong intermolecular H-bond between on-mesogenic (DGA) and mesogenic (6OBA) compounds which is responsible for inducing rich phase polymorphism.

5. Conclusion

The DGA+nOBA ($n = 5$ and 6) hydrogen bonded liquid crystal has been designed and characterized. The induced thermochromic effect and nematic schlieren defects have been analyzed and the reason for the same has been reported. The formation of the H-bond between the compounds and the order parameter of the individual mesophase has been experimentally observed and theoretically (DFT) validated. The presence of the disclination in the nematic phase has been experimentally explored together with possible reasons.

In addition, experimental observations have been validated by hypothetical studies (DFT). Also, the designed structure of the double hydrogen bonded LC mixture has been successfully optimized. The possible use of the present HBLC mixtures in optical devices has been reported. The desirable changes in LC parameters and their importance in the HBLC mixtures are also discussed.

Acknowledgments

One of the authors, V.N. Vijayakumar, acknowledges the financial support of the Department of Science and Technology (No. SERB/F/7454/2013-2014, dated February 21, 2014), New Delhi, and the Department of Atomic Energy (No. 34/14/14/2016-BRNS/34039, dated April 22, 2016), the Board of Research in Nuclear Science (DAE-BRNS), TNSCST/RFRS/VR/19/2018-2019/7666, dated June 6, 2019, and infrastructural support provided by the Bannari Amman Institute of Technology, Sathyamangalam.

References

- [1] H.K. Bisoyi, S. Kumar, *Chem. Soc. Rev.* **39**, 264 (2010).
- [2] A. Gowda, L. Jacob, P.D. Singh, R. Douali, S. Kumar, *Chem. Select.* **3**, 6551 (2018).
- [3] K. Yoon-Sok, Wang-Cheol Zi, *Liq. Cryst.* **29**, 369 (2002).
- [4] T. Kato, J.M.J. Frechet, *J. Am. Chem. Soc.* **111**, 8533 (1989).
- [5] M. Okumus, H. Eskalen, M. Sunkurc, S. Ozan, *J. Mol. Struct.* **1178**, 428 (2019).
- [6] A. Rauch, S. Garg, D.T. Jacobs, *J. Chem. Phys.* **116**, 2213 (2002).
- [7] Yucheng Hu, Yang Qu, Pingwen Zhang, *Commun. Comput. Phys.* **19**, 354 (2016).
- [8] P.G. de Gennes, J. Prost, *The Physics of Liquid Crystals*, 2nd ed., Oxford University Press, Oxford 1995.
- [9] I. Dierking, P. Archer, *RSC Adv.* **3**, 26433 (2013).
- [10] G. Min-Jun, D.A. Beller, D.K. Yoon, *Natur. Commun.* **8**, 15453 (2017).
- [11] H. Tsang-Min, K. McCreary, S. Garg, Thein Kyu, *J. Chem. Phys.* **134**, 124508 (2011).
- [12] M. Shi, C. Xu, Z. Yang, L. Wang, S. Tan, G. Xu, *J. Mol. Struct.* **1182**, 72 (2019).
- [13] R. Kulcar, M. Friskovec, N. Hauptman, A. Vesel, M.K. Gunde, *Dyes Pigm.* **86**, 271 (2010).
- [14] Y. Xu, J. Li, W. Hu, G. Zou, Q. Zhang, *J. Coll. Interface Sci.* **400**, 116 (2013).
- [15] N. Abdullah, A. Rahim Abu Talib, A. Aziz Jaafar, M.A. MohdSalleh, W.T. Chong, *Exp. Therm. Fluid Sci.* **34**, 1089 (2010).
- [16] C.R. Smith, D.R. Sabatino, T.J. Praisner, *Exp. Fluids* **30**, 190 (2001).
- [17] M. Parsley, in: *Proc. SEMI-THERM VII, IEEE 7th Annual Semi-Conductor Thermal Measurement and Management Symp.*, Ed. D. Abbott, Australia 1991, p. 53.
- [18] H.J. Zhou, J.H. Li, S.H. Bao, J. Li, X.Y. Liu, P. Jin, *J. Appl. Surf. Sci.* **363**, 532 (2016).
- [19] S. Zheng, Y. Xu, Q. Shen, H. Yang, *Sol. Energy.* **112**, 263 (2015).
- [20] C.M. Lee, C.P. Jariwala, A.C. Griffin, *Polymer* **35**, 4550 (1994).
- [21] C.M. Lee, A.C. Griffin, *Macromol. Symp.* **117**, 281 (2011).
- [22] L. Onsager, L. Ann, *New York Acad. Sci.* **51**, 627 (1949).
- [23] P. Sheng, in: *Introduction to Liquid Crystals*, Eds. P. Sheng, E.B. Priestley, P.J. Wojtowicz, Plenum Press, New York 1975.
- [24] C. Kavitha, N. Pongali Sathya Prabu, MLN Madhu Mohan, *Physica B Condens. Matter* **407**, 859 (2012).
- [25] R. Rajanandkumar, N. Pongali Sathya Prabu, M.L.N. Madhu Mohan, *Mol. Cryst. Liq. Cryst.* **652**, 111 (2017).
- [26] S. Sundaram, R. Jayaprakasam, M. Dhandapani, T.S. Senthil, V.N. Vijayakumar, *Mol. Liq.* **6243**, 14 (2017).
- [27] S. Malik, P.K. Dhal, R.A. Mashelkar, *Macromolecules* **28**, 2159 (1995).
- [28] G. Varsanyi, *Assignments of Vibrational Spectra of Seven Hundred Benzene Derivatives*, Vols. 1, 2, Adam Hilger, London 1974.
- [29] G.W. Gray, J.W.G. Goodby, *Smectic Liquid Crystals: Textures and Structures*, Leonard Hill, London 1984.
- [30] N.V. Madhusudana, R. Pratibha, *Mol. Cryst. Liq. Cryst.* **103**, 31 (2006).
- [31] F.C. Frank, *Disc. Faraday Soc.* **25**, 19 (1958).
- [32] S. Chandrasekhar, *Liquid Crystals*, Cambridge University Press, Cambridge 1977.
- [33] P.G. de Gennes, *The Physics of Liquid Crystals*, Clarendon Press, Oxford 1974.
- [34] M. Kleman, O.D. Lavrentovich, *Philos. Mag.* **86**, 4117 (2006).
- [35] M. Okumus, *J. Mol. Liq.* **266**, 529 (2018).
- [36] M. Okumus, S. Ozgan, I. Kirik, S. Kerli, *J. Mol. Struct.* **1120**, 150 (2016).
- [37] G.W. Smith, Z.G. Gardlund, *J. Chem. Phys.* **59**, 3214 (1973).
- [38] T. Ranjeethkumar, S. Sundaram, T. Vasanthi, P. Subhasri, T. Chitravel, T.S. Senthil, R. Jayaprakasam, V.N. Vijayakumar, *Braz. J. Phys.* **46**, 649 (2016).
- [39] S. Arulmozhi, M.V.A. Raj, J. Madhavan, *Der. Chim. Sin.* **2**, 158 (2011)
- [40] P.W. Atkins, *Physical Chemistry* Oxford University Press, Oxford 2001.
- [41] K. Fukui, *Science* **218**, 747 (1982).
- [42] R.V. Aghababian, *Essentials of Emergency Medicine*, Jones and Bartlett Publ., 2010.
- [43] T.A. Koopmans, "Über die Zuordnung von Wellenfunktionen und Eigenwertenzuden Einzelnen Elektronen Eines Atoms", *Physica* **1**, 104 (1934).
- [44] C.M. Paleos, D. Tsiourvas, *Angew. Chem. Int. Ed. Engl.* **34**, 1696 (1995).
- [45] M.S. Fedorov, N.I. Giricheva, K.E. Shpil'evaya, E.A. Lapykina, S.A. Syrbu, *Mol. Struct.* **1132**, 50 (2017).